Crystal growth, structural and physical properties of the 5d noncentrosymmetric $LaOsSi_3$*

Zhang Xu(张 旭)[a)b)], Miao Shan-Shan(苗杉杉)[b)], Wang Pu(王 瀑)[b)], Zheng Ping(郑 萍)[b)], Yin Wen-Long(尹文龙)[c)], Yao Ji-Yong(姚吉勇)[c)], Jiang Hong-Wei(姜宏伟)[a)], Wang Hai(王 海)[a)†], and Shi You-Guo(石友国)[b)‡]

[a)] *Department of Physics, Capital Normal University, Beijing* 100048, *China*

[b)] *Beijing National Laboratory for Condensed Matter Physics & Institute of Physics, Chinese Academy of Sciences, Beijing* 100190, *China*

[c)] *Center for Crystal Research and Development, Technical Institute of Physics and Chemistry, Chinese Academy of Sciences, Beijing* 100190, *China*

(Received 10 July 2013; revised manuscript received 2 August 2013)

$LaOsSi_3$ single crystals are synthesized for the first time by an arc melting method. The crystal features a tetragonal $BaNiSn_3$-type structure (space group $I4mm$) which lacks inversion symmetry along the crystallographic c axis and is isostructural with the intensively studied Rashba-type noncentrosymmetric superconductors $LaRhSi_3$ and $LaIrSi_3$. Unlike $LaRhSi_3$ and $LaIrSi_3$ displaying superconductivity, $LaOsSi_3$ shows only metallic behavior over the measured temperature range of 2 K–300 K. The Sommerfeld coefficient γ derived from specific heat is 5.76 $mJ{\cdot}mol^{-1}{\cdot}K^{-2}$, indicating that $LaOsSi_3$ has a weak electronic correlation effect. The absence of superconductivity in $LaOsSi_3$ may lie in the Os 5d bands in the electronic structure. If it is true, it would be useful to provide complementary knowledge in understanding the relation between conduction and the d bands of M in $LaMSi_3$ compounds (M = transition metals).

Keywords: noncentrosymmetric compound, $LaOsSi_3$, structural and physical properties

PACS: 81.05.Zx, 81.10.Fq, 82.75.Fq **DOI:** 10.1088/1674-1056/22/10/108103

1. Introduction

Most superconductors have inversion symmetry in a crystal structure, and the superconducting state can therefore be classified into being either symmetric or antisymmetric (triplet or singlet) paring, because an inversion with respect to the origin in momentum space can at most change the sign of the pair function. By contrast, when the structural inversion symmetry is absent such as in $CePt_3Si$, the pair function will be neither a pure spin-singlet nor a pure spin-triplet pairing but a singlet–triplet mixed state.[1,2] In such a case, the pairing mechanism will be somewhat unconventionally entangled microscopically, showing the different manners for treating spin and orbital parts in the pair function. Specifically, as a result of the absence of inversion symmetry in noncentrosymmetric superconductors, strong antisymmetric spin–orbit interaction (ASOI) will be produced, which will remove spin degeneracy of conduction band and hence the spin and orbital parts of pair function could not be treated independently as those in centrosymmetric superconductors.[3] Moreover, due to the singlet–triplet mixed paring of spins and orbits, the superconducting gap function of a noncentrosymmetric superconductor should be accordingly modified. Furthermore, the ASOI is also capable of splitting the spin-up and spin-down energy bands, thus leading to a split Fermi surface and hence the "unconventional" Cooper pair formed by two electrons contributed by different Fermi surfaces corresponding to spin-up and spin-down bands.[4] In order to elucidate the relation between unconventional superconductivity and the breaking of inversion symmetry, noncentrosymmetric superconductors have become a hot research subject in the condensed matter physics. Subsequent to the discovery of superconductivity in $CePt_3Si$, an array of Ce-based analogues including $CeTSi_3$ (T = Co, Ru, Rh, Pd, Os, and Ir),[5,6] $CeMGe_3$ (M = Fe, Co, Rh, and Ir)[7] were discovered and have been intensively studied. The appearance of superconductivity in the vicinity to magnetic orders in these compounds is highly reminiscent of that in iron-based superconductors,[8,9] in which the superconductivity competes or collaborates with a long-range antiferromagnetic (AFM) spin-density wave (SDW). However, magnetism and superconductivity in Ce-based compounds likely arise from itinerant 4f electrons, thus impeding the extraction of exact relation between superconductivity and inversion symmetry breaking. In this regard, those noncentrosymmetric superconductors containing no active f electrons are necessary.

The $AMSi_3$ (A = La, Ca, Sr, Ba; M = Co, Rh, Ir, Ni, Pd, Pt) compounds are isostructual with $CePt_3Si$,[10] whereas the superconducting behaviors are apparently different, not only because of the indispensable role of high pressure in inducing the superconductivity, which, though, is necessary for Ce-based compounds, but also due to the practical absence of magnetic

*Project supported by the National Natural Science Foundation of China (Grant Nos. 11274367, 10904097, and 11274233) and Chinese Academy of Sciences.

†Corresponding author. E-mail: wanghai@mail.cnu.edu.cn

‡Corresponding author. E-mail: ygshi@aphy.iphy.ac.cn

© 2013 Chinese Physical Society and IOP Publishing Ltd

ordering precursory, the superconductivity which indicates a more conventional paring mechanism. Among $AMSi_3$ compounds, $LaRhSi_3$ ($T_c = 2.6$ K) and $LaIrSi_3$ ($T_c = 0.77$ K) can be categorized into the Rashba-type,[11–15] whose inversion symmetry breaking is only along one direction, i.e., the crystallographic c axis. The two compounds exhibit metallic behaviors in their normal state and weak-coupling full-gap behaviors in the superconducting state. However, origins of the different values of T_c in the two compounds remain unclear yet, which likely has a close relation with the d bands of M in the electronic structure. To confirm the hypothesis, more clues from other 4d and 5d analogues are desired. Another candidate of Rashba-type compounds, the 5d $LaOsSi_3$, was reported many years ago whereas its structural and physical properties have not been available up to now due to the difficulty in high-quality sample synthesis. A systematic study on $LaOsSi_3$ towards well understanding the relation between superconductivity and the M metals is necessary, which would be helpful for achieving a generic picture between the superconductivity and the electronic structure of such compounds. In this study, a single crystal of $LaOsSi_3$ is successfully prepared with the arc melting method. The structural and the electronic and magnetic properties are studied by single crystal X-ray diffraction, magnetic susceptibility, isothermal magnetization, resistivity, and specific heat measurements.

2. Experiment

$LaOsSi_3$ crystals were prepared by using the arc melting method in a water-cooled copper hearth, starting from stoichiometric high purity elements, La (3N), Os (4N), and Si (4N). The operation was protected by high purity argon gas. In order to improve the sample homogeneity, the melted sample was turned over and re-melted several times. The weight loss during these procedures was less than 0.3%. The crystals were obtained by extracting the surface of the ingot.

The composition of the crystal was checked by using the energy dispersive X-ray (EDX) equipped on a HITACHI S-4800 scanning electron microscope (SEM). Phase purity was examined by a SHIMADZU XRD-7000 X-ray diffractometer at 296(2) K with Cu $K_{\alpha 1}$ ($\lambda = 1.540596$ Å). X-ray diffraction (XRD) data were recorded in a 2θ range of 10°–80° in steps of 0.02°. The current and voltage used to generate the X-ray were 40 mA and 40 kV, respectively. The single crystal XRD spectrum was measured on a Bruker SMART APEX II diffractometer using Mo K_α radiation ($\lambda = 0.71073$ Å). The software SAINT+ and XPREP were used for data acquisition, extraction/reduction, and empirical absorption correction.[16,17]

The electrical resistivity (ρ) of $LaOsSi_3$ crystal was measured by using a standard four-probe technique with a gauge current of 0.01 mA. Platinum wires and silver paste were used to make electrical contacts. The measurement was conducted by cooling the sample from 300 K to 2 K on a commercial PPMS (Physical Properties Measurement System) from QD (Quantum Design). The specific heat (C_p) was measured by a time-relaxation method between 2 K and 300 K on the same apparatus. About 15.0-mg small crystals were collected for the use. The direct current (DC) magnetic susceptibility (χ) was measured on a commercial instrument consisting of a SQUID (superconducting quantum interference device) magnetometer from QD between 2 K and 300 K in an applied magnetic field of 50 kOe (1 Oe = 79.5775 A·m^{-1}). The zero field-cooled (ZFC) and field-cooled (FC) modes were adopted for the measurement. The field dependence of isothermal magnetization was measured between +50 kOe and −50 kOe at 2 K and 300 K on the same apparatus. To obtain the accurate information from sample, magnetic moment of the copper sample holder was also measured independently in the same temperature range and eventually deducted from the total magnetization.

3. Results and discussion

A scanning electron microscope image of the typical $LaOsSi_3$ crystal is shown in the inset of Fig. 1. The crystal has a mirror-like smooth surface except for several small stages which may indicate multiple orientations. Typical crystal size is about 800 μm×200 μm×30 μm. Average ratio of the composition derived from EDX characterization is close to nominal composition ratio, implying stoichiometry (or nearly stoichiometry) of the obtained crystal. The single crystal XRD patterns for $LaOsSi_3$ are presented in Fig. 1, showing main c-axis orientation with very sharp Bragg reflections. The major diffraction peaks match well with a tetragonal $BaNiSn_3$-type structure (space group $I4mm$, No. 107). Besides, other peaks possibly arising from unknown impurities are also observed. The calculated lattice parameter c by using Powder X software is about 9.9719 Å.[18]

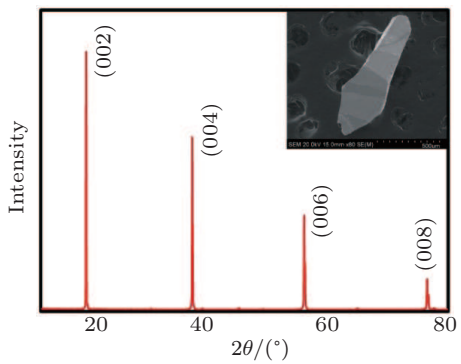


Fig. 1. (color online) Room temperature XRD patterns of the $LaOsSi_3$ crystal with the main Bragg reflection being indexed. Inset shows an SEM picture of a selected crystal.

To obtain more detailed information about the crystal structure of $LaOsSi_3$, structure refinement using the program SHELXL-97[19] by a full-matrix least-square method was performed on basis of single crystal XRD data. The best solutions were achieved by using an initial model of $LaIrSi_3$, and the results are summarized in Tables 1–3. The sufficiently small R factors ($R_F = 0.0561$, $R_w = 0.1445$) guarantee the reliability of the refinement. The yielded lattice parameters are $a = 4.2787(6)$ Å and $c = 9.967(2)$ Å. The obtained lattice constant c is slightly smaller than the value calculated from powder XRD data. The refined occupancy of La is at the 2a site (0, 0, 0.3418(3)); Os is at the 2a site (0, 0, 0.6865(2)); Si(1) at the 2a site (0, 0, and 0.9187(2)); Si(2) at the 4b site (1/2, 0, and 0.5803(3)). The arrangement of the atoms is in good agreement with that in a $BaNiSn_3$-type structure. To show a direct comparison between $LaOsSi_3$ and other $LaMSi_3$ compounds, their lattice parameters are summarized in Table 4. For $LaOsSi_3$, the lattice parameter c is slightly larger than those of other $LaMSi_3$ compounds, which is likely to be due to the different ionic radii between Os and other M elements. The positional parameters, the selected bond distances, and the bond angles obtained using the program STRUCTURE TIDY[19] are also listed in Tables 2 and 3, respectively. Compared with those of other $LaMSi_3$, the values are neither unusually large nor unusually small. Overall, the refinement results indicate that the crystal structure of $LaOsSi_3$ does not vary much as compared with those of other $LaMSi_3$ compounds.

Table 1. Crystal structure refinement results for $LaOsSi_3$.

Empirical formula	$LaOsSi_3$
Formula weight/(g/mol)	413.38
Temperature/K	296 (2)
Wavelength/Å	0.71073
Crystal system	tetragonal
Space group	$I4mm$ (107)
Unit-cell dimensions	
a/Å	4.2787(6)
c/Å	9.967(2)
Cell ratio	$a/b = 1.0000$, $a/c = 0.4293$
Cell volume/Å^3	182.47(2)
Z	2
Calculated density/(g/cm^3)	7.52341
Crystal size/mm^3	0.8×0.2×0.03
μ/cm^{-1}	47.054
$R(F)^a$	0.0561
$R_W(F_o^2)^b$	0.1445
Refinement software	SHELXL-97

[a] $R(F) = \sum||F_o| - |F_c||/\sum|F_o|$ for $F_o^2 > 2\sigma(F_o^2)$.
[b] $R_w(F_o^2) = \{\sum[w(F_o^2 - F_c^2)^2]/\sum wF_o^4\}^{1/2}$ for all data.
$w^{-1} = \sigma^2(F_o^2) + (zP)^2$, where $P = (\mathrm{Max}(F_o^2, 0) + 2F_c^2)/3$.

Table 2. Atomic coordinates of $LaOsSi_3$.

Atom	Wyck.	x	y	z	U_{eq}/Å^2
Os	2a	0	0	0.6865(2)	0.0129(2)
La	2a	0	0	0.3418(3)	0.0092(2)
Si1	2a	0	0	0.9187(2)	0.0065(7)
Si2	4b	1/2	0	0.5803(3)	0.0162(7)

Table 3. Selected bond distances and bond angles of $LaOsSi_3$.

Bonds	Bond distance/Å	Bonds	Bond angle/(°)
Os–Si1	2.313(4) × 1	La–Os–Si1	62.91(2)
Os–Si2	2.387(6) × 4	La–Os–Si2	68.8(2)
La–Si1	3.121(4) × 4	Si1–Os–Si2	116.3(3)
La–Si2	3.199(10) × 4		
La–Os	3.398(2) × 4		

Table 4. Values of lattice parameters, electronic specific coefficient γ, and superconducting transition temperature T_c in $LaTSi_3$ ternary system (T = Os, Rh, Pd, Ir) with the $BaNiSn_3$-type structure.

Compound	a/Å	b/Å	γ/mJ·mol^{-1}·K^2	Θ_D/K	T_C	Reference
$LaOsSi_3$	4.2787	9.967	5.76	375		This work
$LaRhSi_3$	4.2693	9.8292	6.04	357	2.16	Ref. [10]
$LaPdSi_3$	4.352	9.661	5.3	354	2.6	Ref. [14]
$LaIrSi_3$	4.278	9.83	4.5	225	0.77	Refs. [1] and [11]

The structural view of $LaOsSi_3$ based on the refined parameters is schematically drawn in Fig. 2. The network is constructed in a similar manner to $BaNiSn_3$, which lacks a mirror plane. A two-fold axis is normal to the crystallographic c axis (z axis). The crystal structure can be basically described by a sequential arrangement of the La–Os–Si(1)–Si(2)–La–Os–Si(1)–Si(2)–La planes along the c axis. The stacking structure could be compared with other two known body-centered-tetragonal structures, i.e., $ThCr_2Si_2$- (space group: $I4/mmm$) and $CaBe_2Ge_2$-types (space group $P4/nmm$), whose stacking sequences are Th–Cr–Si–Cr–Th and Ca–Ge–Be–Ge–Ca, respectively. The structure of $LaOsSi_3$ can therefore be regarded as an ordered variant of the centrosymmetric $ThCr_2Si_2$-type structure. Since the structure of $BaNiSn_3$-type was already intensively studied previously,[20] it will not be discussed in detail herein.

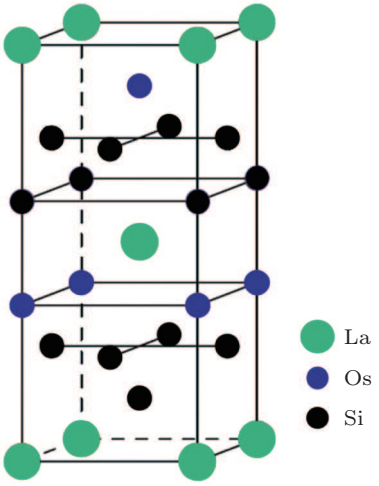


Fig. 2. (color online) A structural view of $LaOsSi_3$.

Figure 3 shows the temperature-dependent $\rho(T)$ of $LaOsSi_3$ in a temperature range between 2 K and 300 K. Unfortunately, no superconductivity was detected with cooling down even to 2 K. Instead, the $\rho(T)$ displays a monotonic decrease upon cooling, indicating a metallic behavior ($d\rho/dT > 0$). It is obvious that the room temperature resistivity $\rho(300\ \mathrm{K})$ is rather small, which is only $\sim 28.44\ \mu\Omega\cdot$cm. A close inspection to the $\rho(T)$ data can reveal an almost saturation behavior of $\rho(T)$ below 10 K with a nearly constant value of about 1.875 $\mu\Omega\cdot$cm. We plot the $\rho(T)$ data by using the Fermi-liquid model with the formula $\rho(T) = \rho_{01} + AT^2$. Satisfying plot could be achieved only above 230 K, which is shown in the inset of Fig. 3, revealing a non-Fermi-liquid behavior at low temperature. Instead, similar to other analogues, the $\rho(T)$ of $LaOsSi_3$ can be well described by the conventional Bloch–Grüneisen (BG) model[21,22] with the formula

$$\rho(T) = \rho_{02} + \left(\frac{4C}{\Theta_D}\right)\left(\frac{T^5}{\Theta_D^5}\right)\int_0^{\Theta_D/T} \frac{x^5\,dx}{(e^x-1)(1-e^{-x})}, \quad (1)$$

where ρ_{02} is the residual resistivity arising from static defects in the crystal lattice as well as the spin-disorder resistivity due to the disordered magnetic moments, C is the electron–phonon interaction constant, and Θ_D is the Debye temperature. In Fig. 3, the fitted curve is presented by empty squares. The fitting gives $\rho_{02} = 1.87\ \mu\Omega\cdot$cm and thus the yielded residual resistivity ratio

$$RRR = \rho(300\ \mathrm{K})/\rho(2\ \mathrm{K})$$

is approximately 15, indicative of high-quality of $LaOsSi_3$ crystal and a good metallic conduction. Overall the features show that the behaviors of $\rho(T)$ highly resemble those generally observed in other centrosymmetric superconductors in the normal state, indicating a basically similar dominated conduction mechanism. Considering that many similarities between $LaOsSi_3$ and other $LaMSi_3$, the $LaOsSi_3$ might have a smaller superconducting transition temperature below 2 K. A further check by a measurement at low temperature remains necessary.

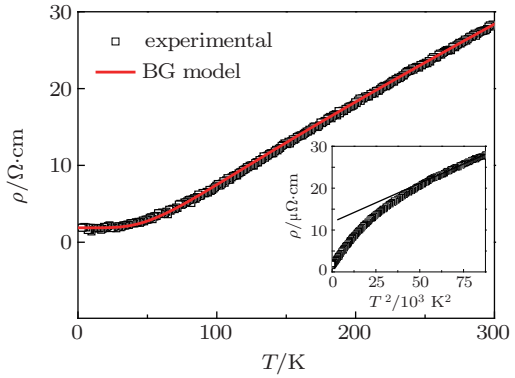


Fig. 3. (color online) Plots of electrical resistivity ρ of $LaOsSi_3$ versus temperature T measured in zero magnetic field. The solid line represents the fitted result by using the Bloch–Grüneisen model. The inset shows a plot by using the Fermi-liquid model.

The $\chi(T)$ of $LaOsSi_3$ measured in a magnetic field of 50 kOe is depicted in Fig. 4, and the magnetization is apparently very weak over the measured temperature range. The value of χ(2 K), for example, is only about 1.3×10^{-4} emu·mol^{-1}·Oe^{-1}. There is no visible difference between the ZFC and FC curves. These facts indicate that the $LaOsSi_3$ is not magnetically active. The $\chi(T)$ displays a typical paramagnetic behavior without showing any anomalies signifying the magnetic orderings, which can be further confirmed by failing to plot the reciprocal $\chi^{-1}(T)$ according to the Curie–Weiss law. The isothermal magnetization $M(H)$ data collected at 2 K and 300 K are presented in Fig. 5. Though an "S" shape profile is observed at 2 K, no obvious hysteresis loop is visible, and the curve becomes almost linear at 300 K. The negative $\chi(T)$ above 60 K, as well as the drop of $M(H)$ at high magnetic fields, might arise from impurities which were actually detected by the single crystal XRD.

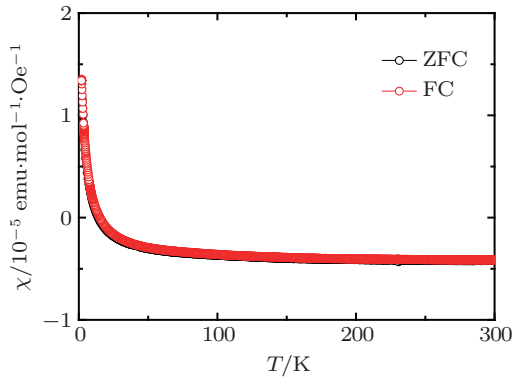


Fig. 4. (color online) Plots of magnetic susceptibility χ versus T of $LaOsSi_3$ measured in 50 kOe.

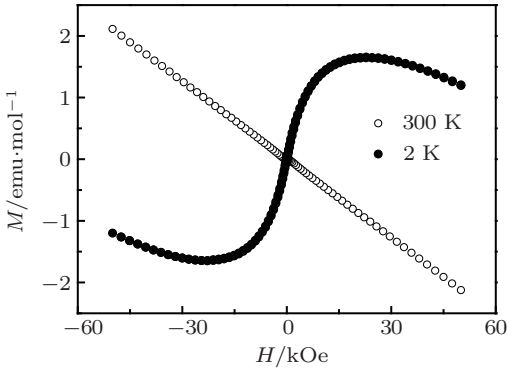


Fig. 5. Values of the field-dependent isothermal magnetization M of $LaOsSi_3$, measured at 2 K and 300 K, respectively.

To extract more information about the measured magnetization, the nonmagnetic metal model is used for the analysis which is expressed by

$$\chi = \chi_{\text{core}} + \chi_{\text{p}} + \chi_{\text{L}}, \tag{2}$$

where χ_{core} represents the diamagnetic term generated by the core electrons, χ_{P} is the bare Pauli paramagnetic spin susceptibility of conduction electrons, and χ_{L} is the Landau–Peierls diamagnetic susceptibility from orbital motion of conduction electrons. The χ_{core} is about -2.12×10^{-4} emu·mol^{-1} obtained from the atomic diamagnetic value in Ref. [23], and $\chi_{\text{P}} = \mu_{\text{B}}^2 N(E_{\text{F}}) \approx 7.77 \times 10^{-5}$ emu·mol^{-1} in Ref. [24], where μ_{B} is the Bohr magnetron and $N(E_{\text{F}})$ could be derived from measured specific heat presented later. The χ_{L} can be estimated from the following relation:[25]

$$\chi_{\text{L}} = -\frac{1}{3}\left(\frac{m_{\text{e}}}{m^*}\right)^2 \chi_{\text{P}}, \tag{3}$$

where m_{e}/m^* is set to be 1, thus giving $\chi_{\text{L}} = -2.59 \times 10^{-5}$ emu·mol^{-1}. The sum of χ_{core}, χ_{P}, and χ_{L} is -1.61×10^{-4} emu·mol^{-1} at 2 K. This value is apparently smaller than the experimental one, indicating other contribution source, most likely from the impurities.

The practical absence of magnetic orders and structural transitions can also be demonstrated by the $C_{\text{p}}(T)$ of $LaOsSi_3$ presented in Fig. 6. The C_{p}(300 K) is approximately 115 J·mol^{-1}·K^{-1}, close to the value estimated from the classical Dulong–Petit heat capacity $C_{\text{p}} = 3nR \approx 124.7$ J·mol^{-1}·K^{-1} for $LaOsSi_3$,[25] where $n = 5$ is the number of atoms per formula unit and R is the molar gas constant. The $C_{\text{p}}(T)$ changes rather monotonically with the decrease of temperature without showing anomalies caused by magnetic and structural transitions. The inset shows the $C_{\text{p}}(T)/T$ versus T^2 plot of the low temperature data in both $H = 0$ and 70 kOe. The linear dependences for all specimens are well within a Debye approximation. Furthermore, the two sets of data coincide very well, also indicative of a nonmagnetic nature of $LaOsSi_3$.

In a low temperature limit, far below the Debye temperature, the Debye function can be approximated as

$$\frac{C_{\text{v}}}{T} = \gamma + \left(\frac{12\pi^4 n N_{\text{A}} k_{\text{B}}}{5\Theta_{\text{D}}^3}\right) T^2, \tag{4}$$

where C_{v}, n, and γ are the heat capacity at constant volume, the number of atoms per formula unit, and the Sommerfeld coefficient, respectively. Good agreement can be achieved by applying Eq. (4) to C_{p}/T versus T^2 plot as can be seen in the inset of Fig. 6. The plots yield $\gamma = 5.76$ mJ·mol^{-1}·K^{-2}, indicating finite density of states (DOS) at the Fermi level, and the electron correlation in $LaOsSi_3$ is not very strong. The γ value is comparable to those of $LaRhSi_3$ and $LaPdSi_3$, 6.04 mJ·mol^{-1}·K^{-2} and 4.5 mJ·mol^{-1}·K^{-2}, respectively.[4,13] Moreover, the yielded Debye temperature Θ_{D} is 375 K, which is also comparable to those of $LaRhSi_3$ and $LaIrSi_3$ listed in Table 3, 357 K and 354 K, respectively.[4,13] With the derived Sommerfeld coefficient γ, the DOS at the Fermi energy $N(E_{\text{F}})$ for both spin directions can be estimated by

$$\gamma = \frac{\pi^2}{3} k_{\text{B}}^2 N(E_{\text{F}})(1 + \lambda_{\text{ep}}), \tag{5}$$

where λ_{ep} is the electron–phonon coupling constant.[24] At a first approximation, $\lambda_{\text{ep}} = 0$ and $N(E_{\text{F}})$ is about 2.41 states/(eV·f.u.).

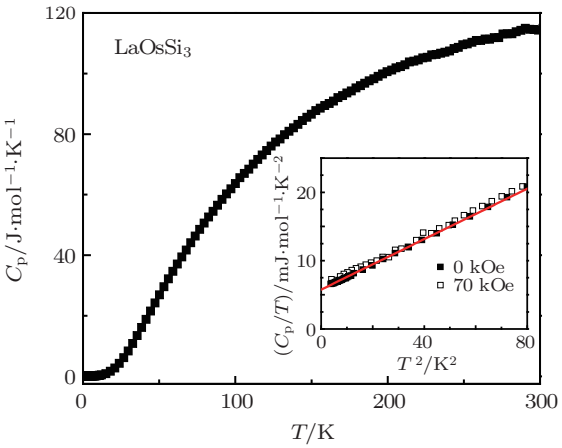


Fig. 6. (color online) The temperature-dependent heat capacity C_p of $LaOsSi_3$. Inset shows the plots of C_{p}/T versus T^2 plot of the data measured in both zero and 70 kOe magnetic fields. The solid lines represent the least-squares fitting of the data using Eq. (4).

According to previous theoretical calculations on $CaIrSi_3$ and $CaPtSi_3$,[26] the spin–orbit coupling likely plays a minor role in determining the transport properties, and the near-Fermi valence bands are primarily derived from the (Ir, Pt) 5d states with a mixture of Si states. Considering many similarities between $LaOsSi_3$ and the two compounds, the conclusion should be also valid in $LaOsSi_3$. Furthermore, it is also proposed that despite of a similar band structure, due to the increased valence electron count and a more localized nature of Pt 5d band, T_{c} of $CaPtSi_3$ (2.3 K) is smaller than that of $CaIrSi_3$ (3.6 K). Within such a framework, $LaOsSi_3$ should

have a higher T_c because the Os band is more itinerant and the valence electron count is smaller. However, as listed in Table 4, the highest T_c of the La-based series appears in $LaPdSi_3$ whose γ is however not smallest. These facts possibly indicate that T_c of the LaMSi$_3$ series does not strongly depend on the valence electron count as what happened in CaMSi$_3$. On the other side, considering that $LaPdSi_3$ ($T_c = 2.6$ K) and $LaRhSi_3$ ($T_c = 2.16$ K) have higher T_c values than $LaIrSi_3$ ($T_c = 0.77$ K) and $LaOsSi_3$ ($T_c < 2$ K or not superconducting), the superconductivity possibly strongly correlates with the d bands of transition metals M. The exact relation between the superconductivity and the M bands in the electronic structure of LaMSi$_3$ should be further systematically investigated to obtain more decisive conclusions.

4. Conclusions

In this paper, $LaOsSi_3$ crystal is synthesized for the first time using the arc melting method. Single crystal X-ray diffraction characterization confirms the tetragonal $BaNiSn_3$-type structure with lattice parameters $a = b = 4.2787(6)$ Å and $c = 9.967(2)$ Å. Resistivity measurements reveal a metallic behavior in the temperature range of 2 K–300 K of the crystal. Magnetization characterizations indicate that the magnetic ground state is essentially paramagnetic. The estimated Sommerfeld coefficient (5.76 mJ·mol^{-1}·K^{-2}) and Debye temperature (375 K) are all comparable to those parameters of other LaMSi$_3$ analogues. The lack of superconductivity in $LaOsSi_3$ over the measured temperature range possibly originates from the Os 5d bands in the electronic structure, and further theoretical calculations on its band structure would be helpful for yielding useful insights into the properties of $LaOsSi_3$.

Acknowledgments

We are grateful to Guo Yan-Feng and Cheng Bing for helpful comments and discussion.

References

[1] Bauer E, Hilscher G, Michor H, Paul Ch, Scheidt E W, Gribanov A, Seropegin Yu, Noël H, Sigrist M and Rogl P 2004 *Phys. Rev. Lett.* **92** 027003
[2] Lejay P, Higashi I, Chevalier B, Etourneau J and Hagenmuller P 1984 *Mater. Res. Bull.* **19** 115
[3] Muro Y, Eom D, Takeda N and Ishikawa M 1998 *J. Phys. Soc. Jpn.* **67** 3601
[4] Anand V K, Hillier A D, Adroja D T, Strydom A, Michor M H, McEwen K A and Rainford B D 2011 *Phys. Rev. B* **83** 064522
[5] Yasuda T, Shishido H, Ueda T, Hashimoto S, Settai R, Takeuchi T, Matsuda T D, Haga Y and Ōnuki Y 2004 *J. Phys. Soc. Jpn.* **73** 1657
[6] Takeuchi T, Yasuda T, Tsujino M, Shishido H, Settai R, Harima H and Ōnuki Y 2007 *J. Phys. Soc. Jpn.* **76** 014702
[7] Shimoda T, Okuda Y, Takeda Y, Ida Y, Miyauchi Y, Kawai T, Fujie T, Sugitani I, Thamizhavel A, Matsuda T, Haga D Y, Takeuchi T, Nakashima M, Settai R and Ōnuki Y 2007 *J. Magn. Magn. Mater.* **310** 308
[8] de la Cruz C, Huang Q, Lynn J W, Li J Y, Latcliff W II, Zarestky J L, Mook H A, Chen G F, Luo J L, Wang N L and Dai P C 2008 *Nature* **453** 899
[9] Rotter M, Tegel M and Johrendt D 2008 *Phys. Rev. Lett.* **101** 107006
[10] Bauer E, Khan R T, Michor H, Royanian E, Grytsiv A, Melnychenko-Koblyuk N, Rogl P, Reith D, Podloucky R, Scheidt E W, Wolf W and Marsman M 2009 *Phys. Rev. B* **80** 064504
[11] Agterberg D F and Kaur R P 2007 *Phys. Rev. B* **75** 064511
[12] Kimura N, Ito K, Saitoh K, Umeda Y, Aoki H and Terashima T 2005 *Phys. Rev. Lett.* **95** 247004
[13] Okuda Y, Miyauchi Y, Ida Y, Takeda Y, Tonohiro C, Oduchi Y, Yamada T, Dung N D, Matsuda T D, Haga Y, Takeuchi T, Hagiwara M, Kindo K, Harima H, Sugiyama K, Settai R and Onuki Y 2007 *J. Phys. Soc. Jpn.* **76** 044708
[14] Settai R, Miyauchi Y, Takeuchi T, Lévy F, Sheikin I and Ōnuki Y 2008 *J. Phys. Soc. Jpn.* **77** 073705
[15] Anand V K, Adroja D T, Hillier A D, Taylor J and Andŕe G 2011 *Phys. Rev. B* **84** 064440
[16] SAINT, version 7.60A; Bruker Analytical X-ray Instruments, Inc. Madison, WI, 2008
[17] Sheldrick G M 2008 *Acta Crystallogr. Sect. A* **64** 112
[18] Dong C 1999 *J. Appl. Cryst.* **32** 838
[19] Sheldrick G M 1997 *SHELX-97 Program for Crystal Structure Refinement*, University of Göttingen, Germany
[20] Kimura N, Muro Y and Aoki H 2007 *J. Phys. Soc. Jpn.* **76** 051010
[21] Huang G, Greenblatt M and Croft M 1989 *Eur. J. Solid State Inorg. Chem.* **26** 193
[22] Blatt F J 1968 *Physics of Electronic Conduction in Solids* (New York: McGraw-Hill)
[23] Mendelsohn L B, Biggs F and Mann J B 1970 *Phys. Rev. A* **2** 1130
[24] Kittel C 1966 *Introduction to Solid State Physics*, 4th edn. (New York: Wiley)
[25] Wagner D 1972 *Introduction to the Theory of Magnetism*, translated by Ferdinand Cap Translation, ed. Terhaar D (Oxford: Pergamon) p. 31
[26] Perrier Ch, Kreisel J, Vincent H, Chaix-Pluchery O and Madar R 1997 *J. Alloys Compd.* **262–263** 71